KnE Materials Science

Knowledge E
Engaging minds

Conference Paper

Physio-mechanical Materials Testing Using Scanning Contact Potentiometry Method

A. A. Abu Ghazal, P. S. Dzhumaev, A. V. Osintsev, V. I. Polski, and V. I. Surin

National Research Nuclear University MEPhI (Moscow Engineering Physics Institute), Kashirskoe shosse 31, Moscow, 115409, Russia

Abstract

To study the processes of forming and growing embryonic fatigue cracks in steel EI-847 when tested under a uniaxial tension at constant load; adapting the method of scanning contact potentiometry using the INSTRON-5982 machine. The embryo was detected on the sample surface- in the yield point- and stably tracked by the equipment indications at higher loads up to the fracture point.

Keywords: scanning contact potentiometry, electrical non-destructive testing, tension testing, fatigue crack, time-frequency signal analysis.

🔓 **OPEN ACCESS**

1. INTRODUCTION

Seamless cold-deformed thin-walled pipes at high temperature corrosion-resistant austenitic steels 06H16N15M3B (EI-847; TY 14-159-293-2005) are used as a fuel element shell in nuclear power plants, it is also considered a candidate in the absorbing element construction, at a temperature between 900–1200 °C, with a combined absorber B_4C-Hf for regulators in VVER-1000 reactors[1]. Experience shows that using corrosion-resistant steel in nuclear reactors for a long-term operation leads to an occurrence and a development of a various types of damage, due to working stresses arising from the pressure and temperature of the operational environment. At present, a highly serious issue of a safe operation of PGV-1000M steam generators in the VVER-1000 reactor system is the stress-corrosion cracking in the welded joint node No. 111 [2]. When microscopic cracks or discontinuities appear in this node, a further operation of the steam generator can lead to its destruction. Therefore, the early stage solution for detecting mechanical defects will guarantee the operation safety, and to avoid a high material costs in case of failure.

Nowadays, there is a list of non-destructive testing methods for nuclear power plant equipments including ultrasonic, acoustic-emission, eddy current, magnetic anisotropy, and others.

Use scanning contact potentiometry (SCP) method opens up opportunities to study surface stresses distribution and deformations, mechanisms of plastic deformation, stages of development of internal defects leading to material destruction, and other physical processes. An informative electrical signal is formed on the contact spots of the transducer-the mechanical contact surface is a sensitive element of the electro-physical transducer-while the object of control is under load.

The number of contact spots of the transducer is determined by the intensity of the contact interaction in the contact zone and the processes occurring in this zone. It also depends significantly on the variation of ripple and roughness parameters. Sensors of Scanning Contact Potentiometry method (SCP), has advantages over other nonde-structive testing measuring devices. The main advantages are: sensitive element has a low weight, small dimensions due to the small linear dimensions of the spots formed under micro contact; high reliability and reproducibility of measurement results; High immunity noise and low noise level.

Sensor design adapted in this method is empty from high-current circuits and heated areas; therefore, measuring system is characterized by high fire safety. Low power level of useful signals and the absence of sparkle in mechanical contacts should also be noticed.

The SCP method provides the possibility of multi-point and distributed measurements, including the use of time-frequency multiplexing of sensitive elements located in different portions of the test object. Temporal coding program and spectral analysis were used to process the incoming information flow.

Aims of this work are to study the fatigue failure of steel EI-847 with the SCP method, to establish a causal relationships between the parameters of the diagnostic signal and the structural changes of the material, to study the construction of potentiograph surface for various loads and to study the fractured surfaces of a sample by the method of fractography; by means of both optical and electron microscopy.

2. RESEARCH METHODS

2.1. Scanning contact potentiometry

The results of preliminary tests carried out of the tensile machine P-5 on steel 12H18N10T and steel-45 showed that during the loss of a stable flow and the formation of a local constriction, the most noticeable changes in the amplitude of the electric potential difference occurring at a higher speed are observed in the region of local narrowing and are connected, in particular, with the processes of forming a cup

fracture and the nucleation of a microscopic crack. For austenitic steels, higher signal amplitude was detected in the load region corresponding to the short-term tensile strength. The obtained results allowed the correcting of the fatigue testing technique, to determine the frequency-time intervals of the change in the useful signal and to develop additional programs for processing and presenting the results.

Potentiometric measurements were performed using the hardware-software complex "*ElphysLAB-IDS*" of the mobile information-diagnostic system located in the Asus X554L laptop. To perform measurements in the manual detection mode, a programmable amplitude discriminator (PAD) of measuring signals with adjustable amplitude discrimination scale in the range of 40 dB was developed. The purpose of the discriminator is to cut off those signal amplitude values that are higher than the set level, which makes it possible to investigate the distribution of the electric potential at different scales. Narrowband filter allows you to adjust the PAD amplitude, starting at the level of tenths of microvolt's, with 0.1 µV step, wideband from units to tens of mV. The measuring system is controlled by the Windows OS and the sampling rate is 1 Hz. Flat samples of steel EI-847, $170 \times 50 \times 2$ mm, were made by milling from sheet metal with subsequent working surface polishing to a roughness of R_a = 0.3 µm. To measure the electric potential difference, sensors with electro-physical converters made of copper M-2 and low-carbon steel St3 were used. Mechanical movement of the sensor along the surface of the sample was carried out along eight measuring tracks, four of which belonged to the left side of the sample (relative to the longitudinal axis of symmetry) and four to the right. The length of the track was about 90 mm, and the distance between tracks was $\sim$ 3 mm. With an average scanning speed of 5 mm / s, the time of one set of measurements varied within two minutes interval. During the tests -increasing the load-a mosaic pattern of changes in surface potentials, related to the manifestation of dynamic waviness and roughness, was observed on the potentiograms. Tensile tests were carried out on an electromechanical tensile testing machine INSTRON-5982 during the process testing and recorded a stress–strain curve of the sample. The load was increased stepwise when converted to a stress of $\sim$ 30-50 MPa after each current test regime. Each cycle with a predetermined load values was terminated by a complete unloading of the sample, a change in its shape was recorded and the roughness on the working surface was measured. Within one week after the tests, the sample was kept in an unloaded state under normal conditions, after which the tests were resumed, starting-as a rule- from a higher load level. During the experiment, at each regime, sample surface temperature was measured using thermocouple. In total, five test cycles were conducted in stress range from 12 to 680 MPa as shown in Table 1.

Table 1: Specifications of electromechanical testing using INSTRON-5982.

Statistical load, kN	up to 100
The resolution of the servo to move, µm	0.08
Accuracy of displacement measurement from measured value,%	±0.05
Test speed, mm/min	0.005-1016
The accuracy of the drive speed of set, %	±0.05
Frequency of synchronous data recording, kHz	1

2.2. Optical and Electron Microscopy

The fracture surface of the sample was studied by both optical and electron microscopy. Cutting ends for fractographic studies in a scanning electron microscope was performed with a precision cutting machine *MECATOME* T180. The machine allows to process samples of a wide class of materials, has adjustable cutting parameters that are set using a touch screen. After cutting the ends, the samples were filled with conductive Carbon-containing polymer *Technovit* 5000. Pressing samples into the conductive composition before polishing was carried out using the XQ-2B molding press. Thin section for studies were prepared using semi-automatic grinding and polishing machine *POLYLAB* P12 and preliminary stages of surface preparation were performed. For final polishing, an alkaline suspension of colloidal silica SiO_2 with a particle dimension of 50 nm was used. To control the quality of the sample surface during grinding, an optical metallographic microscope MMP-4 was used. Resulting a roughness corresponded to twelfth grade of surface purity with a R_a parameter equal to 0.04 µm, it did not contain mechanical damages affecting quality of images obtained and results of microanalysis.

2.3. Surface profilometry

To study fracture surface, the optical microscope MBS-1 and MOTIC SMZ-143 were also used. The distribution of ripple and roughness on working surface sample was determined using a universal digital surface roughness tester (VOGEL). The arithmetic mean deviation of the surface profile R_a was measured along eight paths after each test cycle on the basis of 0.25 mm (GOST 2789-73).

2.4. Microhardness measurement

To calculate the surface stress diagram based on the model of interacting surfaces, Micro-hardness values *H were used*, which were measured on a basis of 1 mm, by Vickers method on an HVS-1000 instrument with automatic feeding of an indenter at a load equal to 1 N. The holding time under load was about twenty seconds; at least 30 measurements were taken at each site. The relative error measurement did not exceed 10%, and values of Micro-hardness varied from three to nine thousand MPa.

3. RESULTS AND DISCUSSION

3.1. Results of the distribution of surface potentials

Selected values of the wave vectors (qi) for the simulation of surface deformations wave at the site of contact with a coordinate (x,y)-coinciding with the working surface-obey the condition $q_{min} \leq q_i \leq q_{max}$, where $q_{min} = 2\eth/$, and $q_{max} = 2\eth/L = 10^{-7}$м and $L = 10^{-4}$м. The Degree of surface deformation $_{sur}$ is evaluated on the basis of function, power spectral density $C(q)$ [4] and used in the analysis of surface stresses Eq(1):

$$\epsilon_{sur} \sim \left(\int dq_x \int C(q)\, dq_y \right)^{-1/2} \tag{1}$$

The size of the fractal is taken equal to D_f = 2,2, and the Hurst exponent H = 0,8, the function $C(q)$ is represented in the form $C(q) \sim q^{-2(H+1)}$ [3].

The structure of the diagnostic signal was analyzed at different levels, starting at values of the order of 0.5 μV. Under the sample load, stress concentrators (active defects) appear at different structural levels. Voltages of the first and second kind (by Davidenkov's criterion) most significantly affect the sign and amplitude of the diagnostic signal, while the signal component associated with third-kind stresses is almost always screened. Under load, stress concentrators (active defects) appear at the different structural levels in the sample. Stress of the first and second kind (by Davidenkov's criterion) most significantly affect the sign and amplitude of the diagnostic signal, while the signal component associated with third-kind stresses is almost always screened. To calculate potentiograms, the method of sequential filtering of the signal components at different levels of amplitude-frequency discrimination was used.

Figure (1) shows the fatigue stress-strain diagram for steel EI-847 and fragments of potentiograph of stress concentrator for the respective chart portions.

The embryo microscopic cracks on the potentiogram was first detected at the end of the penultimate test cycle at load of 525 MPa in the yield stress region, then stably
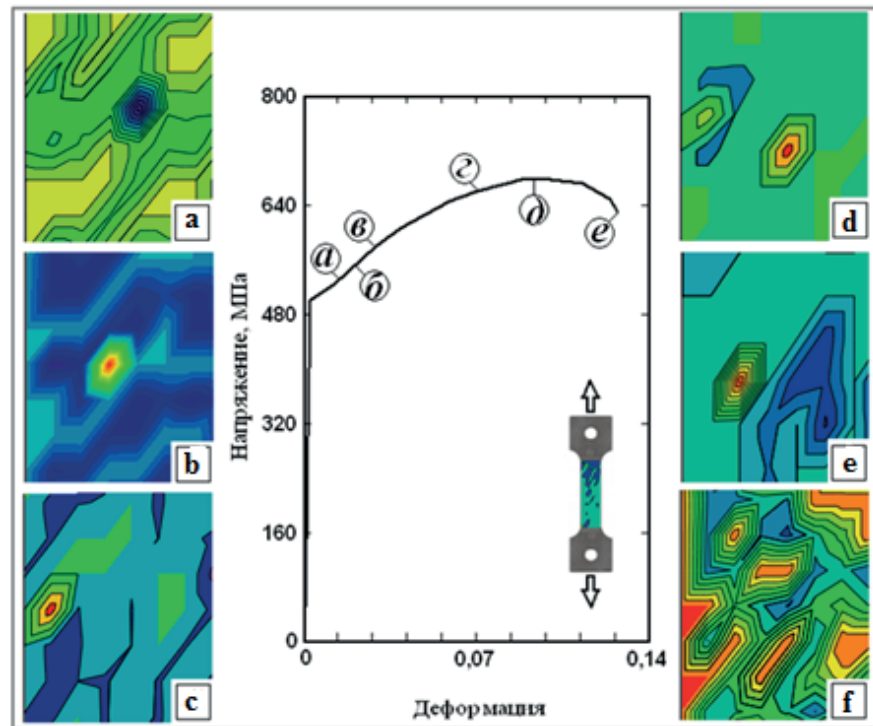
Figure 1: Stress-strain diagram of steel EI-847 (center) and fragments of surface potentiograph of stress concentrator, identified as the embryo is microscopic cracks in the area of localization of the defect.

reproduced on potentiograms in subsequent tests up to failure point. As shown by measurements of the shape and thickness of the sample, the embryo was formed long before the macrolocalization of the plastic flow. On the deformation diagram, the moment of destruction is indicated by the letter (e). The focal point of the destruction was geometrically coincident with the place of appearance of the embryo. The embryo on the potentiogram, like other periodically appearing active defects, has the form of a hexagon elongated along the axis making an angle of ~ 45 degrees with the direction of the applied load. In the center of the hexagon, -at almost all structural levels- from the level of discrimination $(1.10^{-5}$ V) to the level of $(3.7.10^{-4}$ V), there is a region of high positive potential values corresponding to tensile stresses. The potential values gradually decrease in the direction from the center to the boundaries of the hexagon. The embryo on the potentiograms is surrounded by alternating oblique bands (b), by sign to the corresponding compressive stresses, which are near the embryo and oriented at the surface with the same angle close to 45 degrees relative to the direction of the load.

Figure 2 shows the surface potentiograms with the embryo at stress 550 MPa, depending on the choice of discrimination level, manifestedon potentiograms only in a certain range of amplitudes. As follows from the above, with increasing the discrimination, the visible part of the defect grows in size and shifts to the right (b),

and then stretches from the center to the right and moving upwards in the direction indicated earlier (c). With a higher PAD value, the embryo image on the potentiogram disappears.
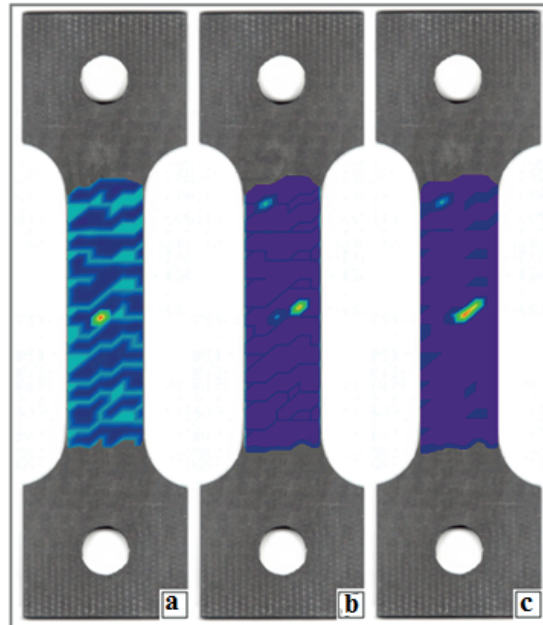
Figure 2: The surface potentiogram of the embryonic crack in the region of defect localization at a stress of 550 MPa, depending on the choice of the PAD range: (a): level of discrimination $1,4 \cdot 10^{-5}$ V; (b): $6,3 \cdot 10^{-5}$ V; (c): $7,9 \cdot 10^{-5}$ V.

Another feature was also found near the yield point and consisted the successive transformation of the region with high stresses surrounding the embryo (Figure 3.a), the appearance of a dipole as shown in (Figure3.b) during the 8-10 minute interval after the load was removed (the PAD level corresponded to 5.10^{-4} V). In Figure 3, the dipole is represented at the mesosteo-logical level (2.10^{-4} V).
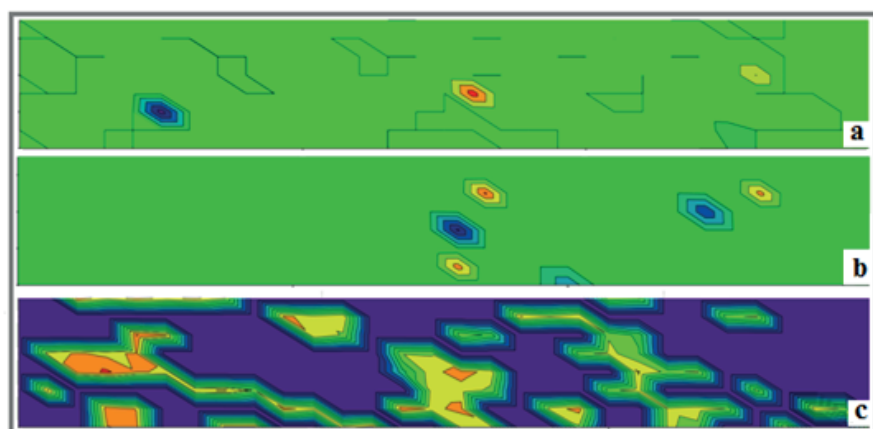
Figure 3: (a): The potentiogram of the embryo in the central part of the sample. (b, c): The appearance of a dipole there with in 10-minutes interval after the removal of the load.

The fracture surface is an oblique cut in cross-section, the greatest thinning with a characteristic tooth on one half of the sample, and the corresponding depression on the other half in the Central part. The size of the tooth along the line of fracture is about two millimeters as shown in (Figure 4), the side surface is parallel to the activities between themselves and perpendicular to the bottom plane of the tooth.

Optical and electron microscopy made it possible to completely reconstruct the pattern of sample destruction. The fractogram of the fracture surface after mechanical tests is a classical viscous fracture over the entire surface of the sample. Multiple pits on the surface of the fracture testify to the formation, growth, and fusion of micro-hollows. The destruction was preceded by a significant plastic deformation of $\sim 13\%$, flowing throughout the volume of the sample and most intensively manifested in the region of the formed neck. The viscous nature of the destruction is confirmed by the presence of a developed grid, the so-called viscous dressings, characterizing this type of failure, which at the microscopic level is due to the substantial hardening of the matrix of the material as a result of cold hardening under cyclic loading. The presence of an insignificant fraction of surfaces that free from viscous dressings (which are more pronounced at the periphery of the fracture) at the fracture is apparently due to the presence of components phase different from the matrix in the material structure, which are characterized by fracture of the type of cleavage along the body of the entire phase separation.
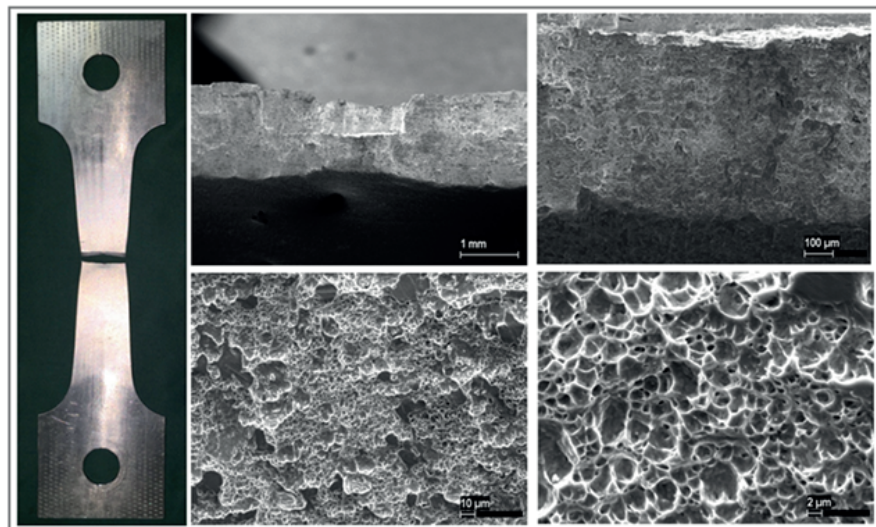
Figure 4: View of the sample after testing (left) and the edge of the fracture region formed at the tooth at different magnifications.

In such a cases, the destruction begins with the formation of micro-snapshots and the merging of micro-voids, which with increasing the load, it actively coalesce. Cracks

in viscous fracture in steels are often formed at the boundary with nonmetallic inclusions and have the appearance of rounded cavities.

Three main stages of fatigue crack development have been identified. At the first, under loads corresponding to the conditional yield point, the embryo was formed in the region of action of the maximum tangential stresses. This region of localization arises as a result of macroscopic stability loss, and this loss is a result of the injection of significant mechanical energy into the system, which leads to an increase in the scale of the plastic deformation fluctuations.

The second stage, the progressive growth of the embryonic fissure is the longest in time, lasting from the moment of detection of the embryo to the destruction of the sample. The amplitude of the electrical potentials in the central part of the sample is increased with increasing the intensity of the applied load, and also it is associated with the increase of the in-homogeneity of the internal stress field around the embryo, as well as the accelerating creep process and the growth of plastic deformation in this region. Thus, at a load of 525 MPa, the maximum value of the amplitude of the diagnostic signal was fixed at a level of 2 mV, at about 591 MPa about 4 mV, and at 650 MPa about six mV.

In the third stage, after the formation of the crack and the localization of the flow in the form of a formed neck, the destruction occurred, which was accompanied by a wide range of amplitudes of electrical potentials, and this indicates the presence of both dynamic roughness and undulation with relatively large lengths of surface waves. With the help of electron microscopy, the average ratio of the length of the surface wave (λ) to its height (h) in the immediate vicinity of the fracture line ($\lambda/h \sim$ several tens is established. The smaller branches of micro-cracks -which are oriented at different angles to the fracture line-are found adjacent to the main crack.

At the pre-destruction stage in the hardened surface layer, a macro-groove is formed in the form of a standing deformation wave along the fracture line as shown in (Figure 5). This region is characterized by higher values of micro-hardness. The relief of the fracture is markedly different from the surface of the sample; it has a larger grain structure, and formations in the form of narrow depressions and micro-deepening.

Under the microscope, the shear deformation bands on the surface of the specimen are also visible as shown in (Figure 6) -the arrows in Figure 6 (b) - which is associated with an inhomogeneous matte surface color. The beginning of the stripes and the most saturated matte color are located in the region of the formed neck. The bands are observed on both halves of the sample, the dull gradient is weaker nearer to the places of fixing the sample in the grippers of the machine. The assumed nature of the bands can be related to the passage of the Chernov-Luders macroband [5].
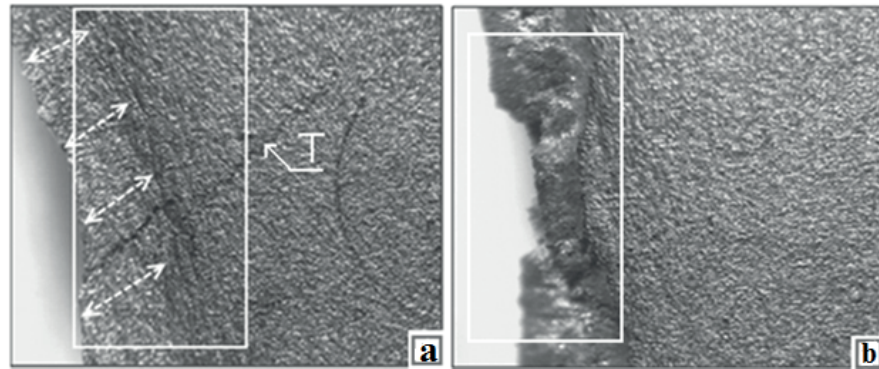
Figure 5: (a): A fragment of the macro-groove near the fracture line is marked with a rectangle and is indicated by two-sided arrows. The same figure shows one of the branching cracks with a length of about 3 mm (denoted by the letter T). (b): Shows the folds in the region of the tooth cavity (an increase of 40x).
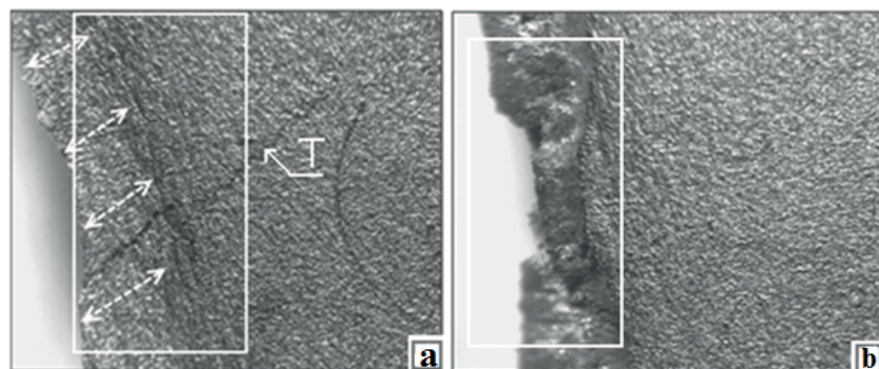

Figure 6: (a): The undulation in the region of the formed tooth. (b): The direction of distribution of the matt bands on the surface after the sample is destroyed.

On the basis of the analysis of potentiograms, which are confirmed by fractographic investigation and roughness measurements, it can be concluded that with increasing the load, the front of plastic deformation moved from the center of the sample to the captures at a speed of several centimeters per hour, while the color of the surface changed with the change in relief. The most noticeable changes in the parameters of dynamic undulation and roughness occurred during the moments of sharp crack growth are shown in (Figure 7).

It should be noted that there is visual similarity between the roughness pattern and the constructed potentiogram at the moment of failure as shown in (Figure 7.b), where the decrease in the roughness values, as well as the potential on the surface, occurs at the center to the periphery. The values of the roughness in the area of failure that are shown in (Table 2), increased more than fourfold as compared with the initial one.

The motion of surface strain waves leads to a chaotic redistribution of stress concentrators. Under the microscope, numerous microbes and pits of different diameters are presented to a greater or lesser extent on the entire surface of the sample and are rounded. At stresses corresponding to the short-term strength limit, a small light

spot several millimeters in size, elongated along the load axis and growing with time, appeared in the region of the embryo. This region is characterized by a high value of plastic deformation with a high density of dislocations. The micro-hardness measured in the zone of strain hardening after the destruction of the sample (the tooth zone) increased almost twofold in comparison with the initial value.
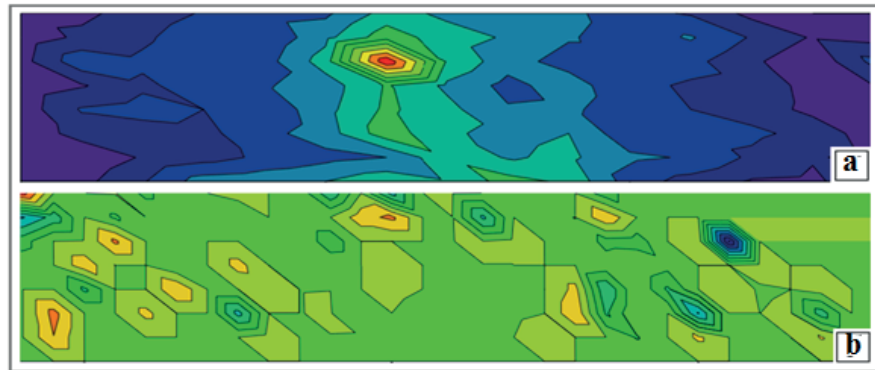
Figure 7: (a): The surface roughness of the sample after its destruction. (b): The surface potentiogram at the moment of failure at a load of 630 MPa.

TABLE 2: Roughness scale (Ra) and electric potential difference ($\Delta\varphi$) on the surface of the sample when it is destroyed.

Color											
$R_a(\mu m)$	1.3	1.2	1.1	1.0	0.9	0.8	0.7	0.6	0.5	0.4	0.3
$\Delta\varphi(mV)$	3.6	2.6	1.6	0.6	0.5	-0.4	-1.4	-2.4	-3.4	-4.4	-6.4

The constructed grid on the potentiograms, with a cell size of 100x100 μm, made it possible to estimate the size of the embryo and its equivalent area. The size of the region corresponding to the maximum tensile stress at the 525 MPa load at the moment of embryo location is from 100 to 200 μm. With increasing the load, the size of the embryo increased by about three times when destroyed. The equivalent area of the embryo was calculated using the formula $S_B = R\lambda = 210^3 \mu m^2$, where R is the radius of the contact spot.

4. CONCLUSIONS

1. In order to further improve the electro-physical diagnosis of a deformation damage, a technique has been developed for detecting discontinuities in a tensile test under conditions close to the ultimate strength. The fatigue failure of EI847 steel by the SCP method was studied and real-time potentiograms were plotted,

the change was monitored by the growth of the fissure nucleus from the time it appeared to the stage of cup fracture formation.

2. The relationship between the parameters of the diagnostic signal and structural changes in the material is established. A consequence of the increase in the signal amplitude during the localization of the current and in the form of a formed neck is the cause of the growth with of a number of contact spots, as well as an increase in the dimensions of the already existing contact spots on the interface of the converter-sample interaction, also the increase of undulation and roughness in the area of the source of destruction. The roughness R_a in the fracture region increased more than fourfold in comparison with the initial values and in the foci of failure corresponded to 1.3 μm. The interaction of protrusions and valleys leads to the formation of localized plastically deformed microscopic regions on the surface, with high values of surface stresses. The current density flowing in such a region depends on the nature of the interaction of the irregularities and the total electrical resistance of the emerging RC-type chains.

3. The result of measuring the dimensions of the area corresponding to the contact spot with the greatest effective stresses at a load of 525 MPa is from 100 to 200 μm on the potentiogram, it characterizes the sensitivity threshold of the detection of the fatigue microscopic crack by the SCP method. The depth of the fracture lies in the interval from a few tenths to 2 millimeters (the thickness of the plate). With increasing the load, the size of the embryo increased by about three times when destroyed. An estimate of the equivalent area of the embryo corresponds to a value of 2.10^3 μm^2. The amplitude of the electric potentials in the central part of the sample increased with increasing the intensity of the applied load and is associated with an increase in the inhomogeneity of the internal stress field around the embryo; at a load of 525 MPa, the maximum value of the amplitude of the diagnostic signal changed at the level 2 mV, at 591 MPa at a level of 4 mV, and at 650 MPa it grew to six mV.

4. Using the method of fractography with the use of electron microscopy, the average ratio of the length of the deformation surface wave to its height in the immediate vicinity of a fracture line equal to several tens is established. The smaller branches of microcracks, which are oriented at different angles to the fracture line, are found adjacent to the main crack, which is also confirmed by the results of spectral analysis.

5. The planned and implemented long three-stage period of destruction of steel EI847 made it possible to obtain a large amount of scientific information that is supposed to be used in the diagnostics of NPP equipment.

References

[1] Krasnorutsky V.S, Belash N.N, Abdullaev A.M. Development and performance characteristics of the scales with an absorber B_4C-Hf. - Issues of atomic science and technology, Year: 2007, № 2, Page: 88-96.

[2] Dub A.V., Durynin V.A, Razygraev A.N. techniques Development of ultrasound testing and determination of the operability of the collector welding station to the PGV-1000M steam generator. - Technical diagnostics and non-destructive testing, Year: 2014, № 4, Page: 36-51.

[3] Greenwood J.A. Constriction resistance and the real area of contact. - Brit. J.Appl.Phys., Year: 1966. Volume: 17. Page: 1621-1632.

[4] Persson B.N.J. Contact mechanics for randomly rough surfaces. - Surf. Sci. Rep., Year: 2006, Volume: 61, Page: 201-227.

[5] Panin V.E., Pleshanov V.S, Burkova S.A. Mesoscopic mechanisms of localization of deformation of low-carbon steel deformed by rolling. - Material Science, Year: 1997, №. 8-9, Page: 22-27.